Scripta Materialia 220 (2022) 114898

Contents lists available at ScienceDirect

Scripta Materialia

journal homepage: www.journals.elsevier.com/scripta-materialia

Physical properties and radiation tolerance of high-entropy pyrochlores $Gd_2(Ti_{0.25}Zr_{0.25}Sn_{0.25}Hf_{0.25})_2O_7$ and individual pyrochlores $Gd_2X_2O_7$ (X= Ti, Zr, Sn, Hf) from first principles calculations

Chenguang Liu [a,*], Qing Peng [d], Tan Shi [e], Fei Gao [c,*], Yuhong Li [b,*]

[a] College of Nuclear Equipment & Nuclear Engineering, Yantai University, Yantai 264005, China
[b] School of Nuclear Science & Technology, Lanzhou University, Lanzhou 730000, China
[c] Nuclear Engineering & Radiological Sciences, University of Michigan, Ann Arbor, MI 48109, United States
[d] State Key Laboratory of Nonlinear Mechanics, Institute of Mechanics, Chinese Academy of Sciences, Beijing 100190, China
[e] School of Nuclear Science and Technology, Xi'an Jiaotong University, Xi'an 710049, China

ARTICLE INFO

Keywords:
First principles
High entropy pyrochlore
Radiation tolerance
Physical properties

ABSTRACT

The physical properties of high-entropy ceramics (HEC) of $Gd_2(Ti_{0.25}Zr_{0.25}Sn_{0.25}Hf_{0.25})_2O_7$ and $Gd_2X_2O_7$ (X = Ti, Zr, Sn, Hf) are investigated using first principles method. The structural properties, anti-site defect energetics, mechanical properties and electronic properties are compared. The lattice constant of HEC is within the range of its constituent pyrochlores, and the local lattice distortion presents in HEC. The cation anti-site defect is much easier to form in HEC than in pyrochlore, which implies that HEC can easily transfer to disordered fluorite structure and exhibit stronger radiation tolerance. The "high entropy" at B site of $A_2B_2O_7$-type pyrochlore had no obvious effect on mechanical properties. The electronic properties of HEC and pyrochlore are characterized by projected density of states distribution and Bader charge, and the causes of HEC lattice distortion are investigated.

Pyrochlore attracted broad attention due to the excellent radiation tolerance and structural and chemical durability. This material was extensively studied for a variety of applications, such as catalyst, optical material, thermal barrier coating and host matrix for high level radioactive waste [1–5]. Pyrochlore with the chemical formula $A_2B_2O_7$ is a derived structure of fluorite structure. The A-site (16c) is located within a distorted cubic polyhedron and typically occupied by lanthanides and actinides. The B-site (16d) is a distorted octahedron and can be occupied by transition metal elements [2,6]. The A and B cations have an eightfold coordination and sixfold coordination with oxygen, respectively. Oxygen ions are located at 48*f*, 8*b* sites and the 8*a* sites in oxygen sublattice are the inherent vacancies. The radius of A and B site cations (r_A and r_B) in pyrochlore is always used to predict the structural stability [7]. When the ratio r_A/r_B is located between 1.46 and 1.78, the structure can maintain a stable pyrochlore phase, otherwise a fluorite phase is favored as the ratio smaller than 1.46 [8].

Due to the robust ability to incorporate actinides and excellent dissolution behavior in natural minerals, pyrochlores are considered to be a potential candidate for the immobilization of high-level nuclear waste [9]. Therefore, some researches focused on the radiation tolerance of pyrochlore naturally [1,10,11]. Particularly, the cation disordering energy is closely correlated with the amorphization resistance in pyrochlore [12]. The cation antisite and anion Frenkel pair defects are the main point defects in pyrochlore, which can result in the transformation from ordered pyrochlore phase to disordered fluorite phase [13]. The atomistic simulation connecting the phase stability of pyrochlore to the defect formation energy has been performed, and the results show that the pyrochlores with smaller r_A/r_B, can form disordered fluorite phase more readily and have relatively small cation anti-site defect formation energy [1,12]. Besides, there are several other factors that also affect the radiation tolerance of pyrochlores, such as bond type in lattice. Lian et al. [14] studied the bond type effect of $Gd_2Sn_2O_7$ and $Gd_2Hf_2O_7$ on the radiation response under 1 MeV Kr^+ irradiation, and the results indicated that the susceptibility to radiation is not only related to radius ratio of cations, but also affected by the covalency of bond type.

High entropy ceramics, including diborides [15], carbides [16], nitrides [17], and metal oxides [18], have been fabricated and attracted wide attention due to their complex compositions, complicated

* Corresponding authors.
E-mail addresses: liuchg@ytu.edu.cn (C. Liu), gaofeium@umich.edu (F. Gao), liyuhong@lzu.edu.cn (Y. Li).

https://doi.org/10.1016/j.scriptamat.2022.114898
Received 24 April 2022; Accepted 27 June 2022
Available online 1 July 2022

microstructures, unique properties and diverse applications. In recent years, a series of reports of high entropy pyrochlore ceramics have sprung up and some of them have been concerned with the low thermal conductivity of high entropy ceramics in the field of thermal barrier coating [19–21]. Besides, Teng et al. [22] studied the process of phase transformation of a large amount of high entropy pyrochlore ceramics and found that the factors affecting phase stability are similar in both high entropy pyrochlores and individual pyrochlores. For example, the average radius ratio is between 1.46 and 1.78, the compounds will maintain pyrochlore phase in both individual pyrochlores and high entropy pyrochlore ceramics [22]. Zhou et al. [9] recommended $(Eu_{1-x}Gd_x)_2(Ti_{0.2}Zr_{0.2}Hf_{0.2}Nb_{0.2}Ce_{0.2})_2O_7$ high entropy pyrochlore as the potential candidate material for immobilizing high level radionuclides waste. They found that the leaching rate of radionuclides in high entropy pyrochlore is much lower than that in $Gd_2Zr_2O_7$ pyrochlore, which is caused by the compositional complexity and lattice distortion in high entropy pyrochlore.

As the aforementioned studies, the high entropy pyrochlores display enhanced physical and chemical properties compared to the individual pyrochlores. To date, there is a lack of a comprehensive comparative analysis of these two types of pyrochlores, and the underlying mechanisms that govern the unique properties of high entropy pyrochlores ceramics have not been fully understood. We chose Gd-pyrochlore as a model representative pyrochlore for our study because it is one of the most important and representative pyrochlores. It has also been proposed as a potential material for immobilizing minor actinides. It possess high neutron capture cross section (2.55×10^5 barns) [23]. We have performed a comparative study of the physical properties and radiation tolerance of high-entropy $Gd_2(Ti_{0.25}Zr_{0.25}Sn_{0.25}Hf_{0.25})_2O_7$ pyrochlore and $Gd_2X_2O_7$ (X=Ti, Zr, Sn, Hf) using first principles calculations. The goal is to explore the mechanisms behind the excellent properties of high entropy pyrochlores at atomistic level.

The Vienna Ab-initio Simulation Package (VASP) [24,25] was used for all the first principles calculations based on the Density Functional Theory (DFT). The projected-augmented-waves (PAW) with the Perdew-Burke-Ernzerhof (PBE) exchange-correlation potentials were adopted [26,27]. The special quasi-random structure (SQS) approach [28,29] was used to generate the high-entropy $Gd_2(Ti_{0.25}Zr_{0.25}Sn_{0.25}Hf_{0.25})_2O_7$ pyrochlores structures with a unitcell of 88 atoms. The Warren-Cowley short range order (SRO) parameter [30] of the high-entropy pyrochlore in this work is zero, which means that the distribution of Ti, Zr, Sn and Hf elements at B-site is random. The SRO is calculated by the following equation: $\alpha_{ij}^{\nu} = 1 - \frac{p_{ij}^{\nu}}{c_j}$, where p_{ij}^{ν} is the probability of appearance of element j around element i in the ν^{th} neighboring shell, and c_j is the atomic concentration of element j. This study was performed with a $2 \times 2 \times 2$ k-point sampling and the plane wave cutoff energy was 600 eV. The atoms in the high-entropy $Gd_2(Ti_{0.25}Zr_{0.25}Sn_{0.25}Hf_{0.25})_2O_7$ pyrochlores and individual $Gd_2Ti_2O_7$, $Gd_2Zr_2O_7$, $Gd_2Sn_2O_7$ and $Gd_2Hf_2O_7$ pyrochlores were fully relaxed and the electronic energy and ionic force convergence criterion were 10^{-6} eV/atom and 10^{-2} eV/Å, respectively. The valence configuration for Gd, Ti, Zr, Sn, Hf and O are $4f^7 5s^2 5p^6 5d^1 6s^2$, $3d^2 4s^2$, $5s^1 5p^0 4d^3$, $4d^0 5s^2 5p^2$, $5d^2 6s^2$ and $2s^2 2p^4$. Gd has strongly correlated $4f$ electrons and the DFT+U method as a correction to the regular DFT method was used to compute the correlation effects. This method has previously been successfully applied to simulate the Gd-pyrochlores [31]. The Hubbard U value for Gd we applied in this work was 4 eV, as proposed by Li et al. [31].

The relaxed lattice structures of HECs and individual pyrochlores are shown in Fig. 1. The lattice constant (a_0), the x parameters for O_{48f}, the bond length in HEC and individual pyrochlores are summarized in Table 1 compared with literature [22,32–38]. The lattice constant for HECs is within the range of its constituent individual pyrochlores. For the x parameter of O_{48f}, a parameter related to the degree of disorder and lattice distortion in pyrochlore, HECs possess the largest value compared with those of all individual pyrochlores. For pyrochlore structure, the x_{O48f} should be between 0.3125 and 0.375 and larger x_{O48f} predicts higher degree of disorder and lattice distortion. The bond lengths in HECs are different from those of all individual pyrochlores, that is, the length of the same type of bonds is different in HECs. For instance, the <Gd-O_{48f}> bond length varies between 2.474 Å and 2.660 Å, as shown in Table 1. The variation of the bond length along with the largest x_{O48f} collectively suggested that there is local lattice distortion in HEC. For clarity, the radial displacement of Gd, Ti, Zr, Sn, Hf and O element based on their positions of perfect lattice was calculated and the results are shown in Fig. 2. The displacement of O atoms is the largest in HEC, followed by Gd atoms, and then Ti, Zr, Sn, and Hf metallic elements. The mixing effect caused by the 3d (Ti), 4d (Zr), 5d (Hf) elements co-occupying B-site of $A_2B_2O_7$ type pyrochlore oxides may result in the

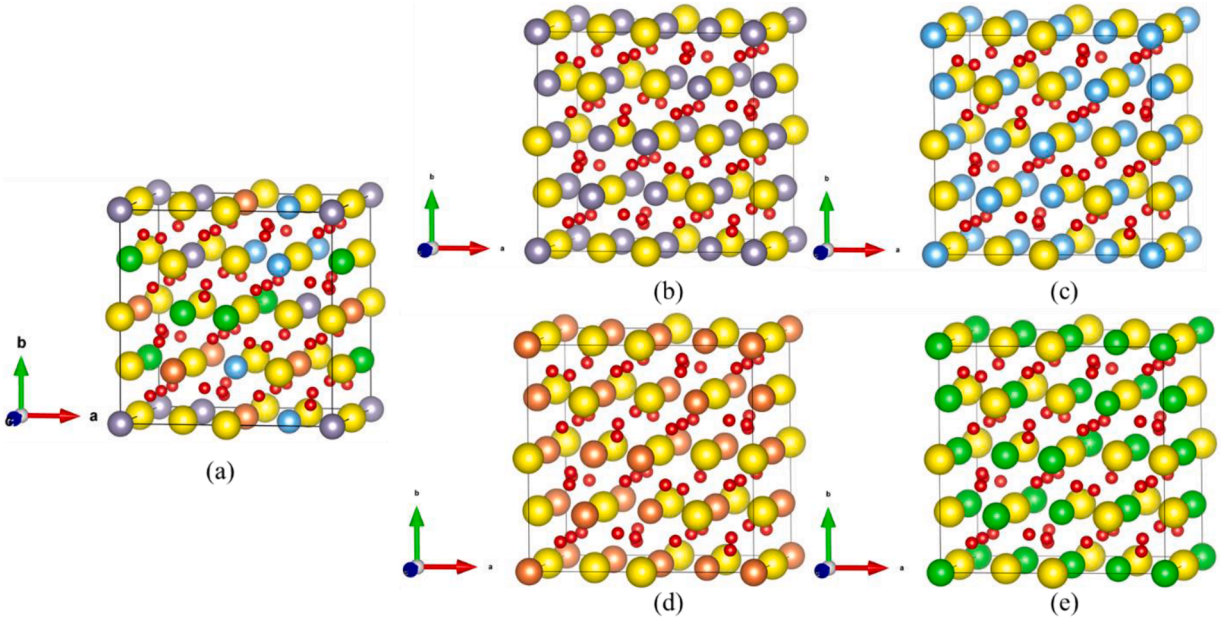

Fig. 1. The relaxed lattice structure of HEC and pyrochlores. (a) $Gd_2(Ti_{0.25}Zr_{0.25}Sn_{0.25}Hf_{0.25})_2O_7$, (b) $Gd_2Sn_2O_7$, (c) $Gd_2Ti_2O_7$, (d) $Gd_2Hf_2O_7$, (e) $Gd_2Zr_2O_7$. The yellow, sky-blue, green, gray and orange spheres represent Gd, Ti, Zr, Sn and Hf atoms, respectively.

Table 1
Calculated lattice constant (a0), the x positional parameter for 48f-site oxygen and bond distance (Å), compared with available experimental and theoretical results.

	a_0 (Å)	x_{O48f}	Gd-O_{48f} (Å)	Gd-O_{8b} (Å)	Ti-O_{48f} (Å)	Zr-O_{48f} (Å)	Sn-O_{48f} (Å)	Hf-O_{48f} (Å)
HEC	10.43	0.350	2.474-2.660	2.221-2.393	1.907-2.114	2.021-2.169	2.025-2.147	2.030-2.240
Ref. [22]	10.44	0.337						
$Gd_2Hf_2O_7$	10.49	0.337	2.520	2.271				2.067
Ref. [32]	10.59	0.340	2.560	2.290				2.080
Ref. [34]			2.534	2.28				2.073
$Gd_2Sn_2O_7$	10.48	0.338	2.513	2.269			2.070	
Ref. [38]	10.54	0.338	2.529	2.283			2.082	
Ref. [33]	10.45	0.335	2.537	2.265			2.048	
$Gd_2Zr_2O_7$	10.56	0.340	2.515	2.286		2.096		
Ref. [37]	10.66	0.339	2.548	2.307		2.110		
Ref. [35]	10.54	0.344	2.483			2.110		
$Gd_2Ti_2O_7$	10.161	0.330	2.496	2.200	1.970			
Ref. [36]	10.195	0.329	2.501	2.207	1.977			
Ref. [36]	10.186	0.327	2.524	2.205	1.961			

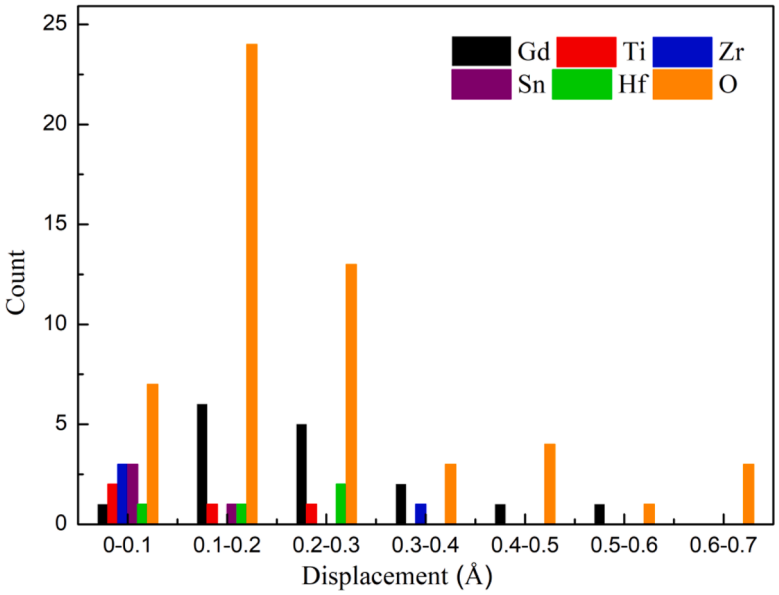

Fig. 2. The radial displacement of each constituent element in HEC.

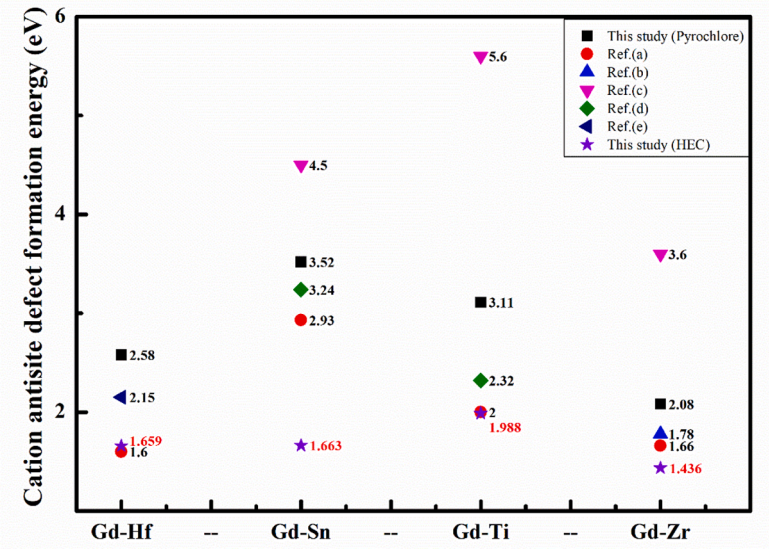

Fig. 3. The calculated cation antisite defect formation energy and available Refs.: (a) [43], (b) [44], (c) [1], (d) [41], (e) [42]. The Gd-Hf, Gd-Sn, Gd-Ti and Gd-Zr represent the cation anti-site defects in HEC and pyrochlores. For example, the Gd-Hf represents the cation anti-site defect by exchanging the Gd and Hf cation in HEC and the corresponding $Gd_2Hf_2O_7$ pyrochlore.

instability of the local microenvironment and then leads to the large displacement.

Moreover, the instability of the local microenvironment will lead to the distortion of A-site cubic polyhedron and B-site octahedron, which can be characterized by the variation of x_{O48f}. It is interesting to note, however, the large displacement of constituent element and local lattice distortion do not cause significant variation of the HEC lattice constant compared with individual pyrochlores, which is also found in high-entropy carbide [39], and demonstrated that the local lattice distortion does not result in lattice expansion, but rather depends on the local chemical environment.

The cation antisite defect formation energy is obtained by Liu et al. [40]:

$$E_f^{CA} = E_{tot}^{CA} - E_{tot} \tag{1}$$

where E_{tot}^{CA} is the total energy of the relaxed pyrochlore or HEC supercells with a cation antisite defect in the lattice, E_{tot} is the total energy of the corresponding ideal lattice. The calculated results and available Refs. [1, 41–44] are summarized in Fig. 3. The black filled squares show the calculated cation anti-site defect formation energy in the pyrochlore of this study. The values are 2.58 eV, 3.52 eV, 3.11 eV and 2.08 eV for $Gd_2Hf_2O_7$, $Gd_2Sn_2O_7$, $Gd_2Ti_2O_7$ and $Gd_2Zr_2O_7$ pyrochlore, respectively. The difference between the calculated results in this study and the reference values is due to the different methods and potentials used in the simulations. The purple filled star in the Fig. 3 show the values of different cation antisite defect formation energies in HEC, which are 1.659 eV, 1.663 eV, 1.988 eV and 1.436 eV for the exchange of Gd and Hf atom, Gd and Sn atom, Gd and Ti atom, Gd and Zr atom in HEC supercells, respectively. The comparison reveals that the cation anti-site defect is more easily to form in HEC lattice than that in individual pyrochlores. This result indicates that the HEC lattice can be easily transformed to disordered fluorite structure, which suggests that HEC pyrochlores exhibit stronger radiation tolerance under radiation [45] according to the cage theory [46,47].

In order to provide a deeper understanding, we have compared the mechanical properties of the individual pyrochlores and HEC. The calculated results with the reference values [31,48–50] are presented in Table 2. The key points can be drawn as the following: C_{11}, C_{12} and C_{44}, three elastic constants for all the pyrochlores and HEC, satisfy the Born ruleiom

$$C_{11} + C_{12} > 0; C_{11} - C_{12} > 0$$

which indicated that all pyrochlores and HEC are mechanically stable. The C_{11}, C_{12} for HEC is comparable to that of $Gd_2Sn_2O_7$ and $Gd_2Zr_2O_7$, but slightly smaller than that of $Gd_2Ti_2O_7$ and slightly larger than that of $Gd_2Hf_2O_7$. The C_{44} for HEC, $Gd_2Hf_2O_7$, $Gd_2Sn_2O_7$ and $Gd_2Ti_2O_7$ is comparable and slightly larger than that of $Gd_2Zr_2O_7$. The bulk modulus B, shear modulus G and Young's modulus can be calculated by using the following formula [51–53]:

$$B = \frac{C_{11} + 2C_{12}}{3} \tag{2}$$

$$G = \left(\frac{C_{11} - C_{12} + 3C_{44}}{5} + \frac{5(C_{11} - C_{12})C_{44}}{4C_{44} + 3(C_{11} - C_{12})}\right) \Big/ 2 \tag{3}$$

$$E = 9BG/(3B + G) \tag{4}$$

The results show that bulk modulus B follows the order of $Gd_2Ti_2O_7$ > $Gd_2Sn_2O_7$ > $Gd_2Zr_2O_7$ > HEC > $Gd_2Hf_2O_7$. For the shear modulus G, the order is $Gd_2Ti_2O_7$ > HEC > $Gd_2Hf_2O_7$ > $Gd_2Sn_2O_7$ >$Gd_2Zr_2O_7$. The order of Yong's modulus E is $Gd_2Ti_2O_7$ > HEC > $Gd_2Sn_2O_7$ ≅ $Gd_2Hf_2O_7$ > $Gd_2Zr_2O_7$. The modulus summarized above demonstrate that the "high entropy" in the B site of $A_2B_2O_7$ pyrochlore has no obvious effect on mechanical properties of pyrochlores. This is because that different elements at the B site weaken the misfit between the coupling force and atom size, and the lattice relaxation will not cause the strain field fluctuation in HEC [40].

Pugh's indicator B/G is associated with the ductility of materials. The critical value to separate brittle and ductile materials is 1.75. If the value is larger than 1.75, the material behaves in a ductile nature, otherwise a brittle nature [54]. Our results and available references are listed in Table 2. The B/G of HEC and pyrochlores are larger than 1.75, which implies that the five materials show a certain ductility.

Poisson's indicator (ν) is another measure of brittleness and ductility of materials. It can be calculated as $\nu = \frac{3B-2G}{6B+2G}$. The material behaves in a brittle nature when ν is around 0.1. If ν is larger than 0.25, the material shows ductile properties [55]. Our calculated results and available references are also listed in Table 2. The value of ν is 0.28, 0.27 0.28, 0.29 and 0.29 for HEC, $Gd_2Hf_2O_7$, $Gd_2Sn_2O_7$, $Gd_2Ti_2O_7$ and $Gd_2Zr_2O_7$, respectively. The Poisson's ratio of HEC and pyrochlores are larger than 0.25, which confirms the conclusion drawn from the Pugh's indicator B/G.

To gain insights into the electronic properties, we have further studied the projected density of states distribution of HEC and individual pyrochlores. The results were shown in Fig. 4. For HEC, the conduction band minimum (CBM) is mainly contributed by Ti 4d and O 2p states. The valence band maximum (VBM) is mainly contributed by O 2p states, the d states of Hf, Sn, Ti and Zr, and the 4f states of Gd. Similarly, for individual pyrochlore, the VBMs are mainly contributed by the d orbitals of elements at B site hybridized with O 2p orbitals and Gd 4f orbitals. The overlap between the d states of metal elements and the p states of O indicates the covalent interactions in HEC. We have calculated the energy band gap individual and HEC pyrochlores. The results were 3.31, 2.81, 2.28, 2.74 and 2.49 eV for $Gd_2Hf_2O_7$, $Gd_2Sn_2O_7$, $Gd_2Ti_2O_7$, $Gd_2Zr_2O_7$, and HEC, respectively, which suggest that these materials share certainly insulating properties.

The Bader charge of each atom in HEC and pyrochlores was calculated and the results were summarized in Table 3. Each atom at different sites of HEC exhibits different Bader charge values, which indicate that four cations occupying at the B sites will result in the different coordination environments and bonding requirements in HEC. The uneven charge distributions and chemical environment may cause the local lattice distortions. The Bader charge of Zr, Sn and Hf atom in HEC and pyrochlores are larger than that of Gd atom, which suggests that the

Table 2
The calculated elastic constants, C_{11}, C_{12}, C_{44}, bulk modulus B, shear modulus G, Yong's modulus E of pyrochlores and HEC. The available references are listed in table. The unit is GPa.

	C_{11}	C_{12}	C_{44}	B	G	E	B/G	ν
HEC	303.29	115.32	93.42	177.98	93.65	239.02	1.90	0.28
$Gd_2Hf_2O_7$	292.26	107.83	93.04	169.31	92.71	235.20	1.83	0.27
Ref. [50]	310.6	105.1	94.7	173.6	97.84	247.1	1.77	0.26
$Gd_2Sn_2O_7$	305.28	119.41	91.14	181.37	91.85	235.76	1.97	0.28
Ref. [49]	300.5	114.6	98.7	176.57	96.37	244.58	1.83	0.27
$Gd_2Ti_2O_7$	323.05	130.41	92.8	194.62	94.19	243.32	2.07	0.29
Ref. [48]	356.8	130.3	110.9	205.8	111.83	284.05	1.84	0.27
$Gd_2Zr_2O_7$	301.38	118.75	86.4	179.63	88.33	227.68	2.03	0.29
Ref. [31]	285.1	102.5	82.1	163.37	85.66	218.76	1.91	0.28

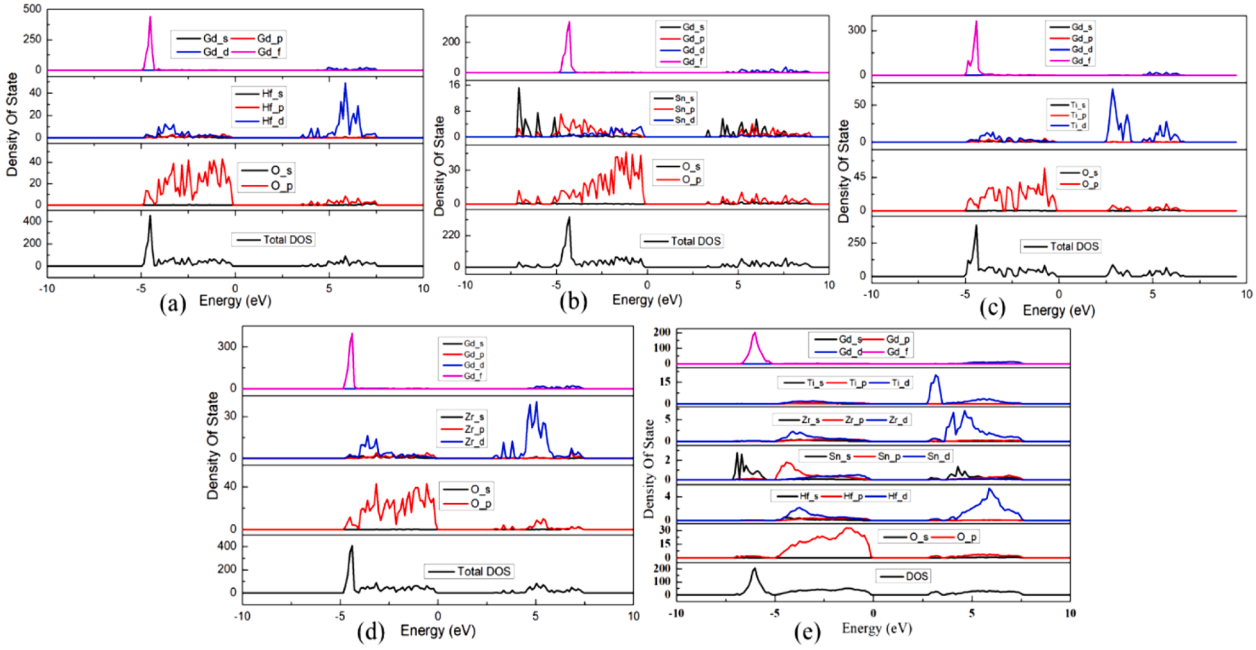

Fig. 4. Projected density of states for (a) $Gd_2Hf_2O_7$, (b) $Gd_2Sn_2O_7$, (c) $Gd_2Ti_2O_7$, (d) $Gd_2Zr_2O_7$ and (e) HEC.

Table 3
The calculated Bader charge (e) for each atom in HEC and pyrochlores.

	Gd	Ti	Zr	Sn	Hf	O
HEC	2.110-1.988	1.983-1.975	2.271-2.235	2.273-2.269	2.333-2.288	1.305-1.153
$Gd_2Hf_2O_7$	2.140				2.313	1.261
$Gd_2Sn_2O_7$	2.135			2.250		1.238
$Gd_2Zr_2O_7$	2.138		2.263			1.295
$Gd_2Ti_2O_7$	2.125	1.957				1.138

ionicity of <Zr-O>, <Sn-O> and <Hf-O> bond is stronger than that of <Gd-O> bond. The Bader charge of Gd atom in both HEC and $Gd_2Ti_2O_7$ pyrochlore is larger than that of Ti atom, which reflects the weaker ionicity of <Ti-O> bond.

In this study, we have presented a first-principles study on the physical properties and radiation tolerance of high-entropy pyrochlore $Gd_2(Ti_{0.25}Zr_{0.25}Sn_{0.25}Hf_{0.25})_2O_7$ and individual pyrochlores $Gd_2X_2O_7$ (X= Ti, Zr, Sn, Hf) within the framework of density functional theory. The structural properties analysis indicates that the lattice constant of HEC is within the range of its constituent pyrochlores and the local lattice distortion presents in HEC. The cation anti-site defect formation energies are used to predict the radiation tolerance. The results suggest that HEC exhibits stronger radiation tolerance than the individual component pyrochlores. The comparation of elastic constants connote that the "high entropy" at the B site of $A_2B_2O_7$-type pyrochlore has no obvious effect on the mechanical properties. The results of electronic properties analysis support the local lattice distortion in HEC, i.e. four cations occupying the B site result in the different coordination environments and bonding environment.

Declaration of Competing Interest

The authors declare no competing interests.

Acknowledgments

This work was supported by the National Natural Science Foundation of China (Grant No. 12175093, 11875046, 11805088.), the start-up fund from Yantai University to C.L. (Grant No. HD20B02.) and Shandong Provincial Natural Science Foundation (Grant No. ZR2021QA028). Q. P. would like to acknowledge the support provided by LiYing Program of the Institute of Mechanics, Chinese Academy of Sciences through Grant No. E1Z1011001.

References

[1] K.E. Sickafus, L. Minervini, R.W. Grimes, J.A. Valdez, M. Ishimaru, F. Li, K. J. McClellan, T. Hartmann, Science 289 (5480) (2000) 748–751.
[2] Z. Wang, G. Zhou, D. Jiang, S. Wang, J. Adv. Ceram. 7 (4) (2018) 289–306.
[3] W.B. Cairncross, D.N. Gresh, M. Grau, K.C. Cossel, T.S. Roussy, Y. Ni, Y. Zhou, J. Ye, E.A. Cornell, Phys. Rev. Lett. 119 (15) (2017), 153001.
[4] M. Zhao, W. Pan, C. Wan, Z. Qu, Z. Li, J. Yang, J. Eur. Ceram. Soc. 37 (1) (2017) 1–13.
[5] B.P. Uberuaga, M. Tang, C. Jiang, J.A. Valdez, R. Smith, Y. Wang, K.E. Sickafus, Nat. Commun. 6 (1) (2015) 8750.
[6] M. Lang, F. Zhang, R. Ewing, J. Lian, C. Trautmann, Z. Wang, J. Mater. Res. 24 (4) (2009) 1322–1334.
[7] J. Lian, K. Helean, B. Kennedy, L. Wang, A. Navrotsky, R. Ewing, J. Phys. Chem. B 110 (5) (2006) 2343–2350.
[8] M.A. Subramanian, G. Aravamudan, G.V. Subba Rao, Prog. Solid State Chem. 15 (2) (1983) 55–143.
[9] L. Zhou, F. Li, J.X. Liu, S.K. Sun, Y. Liang, G.J. Zhang, J. Hazard. Mater. 415 (2021), 125596.
[10] S.A. McMaster, R. Ram, N. Faris, M.I. Pownceby, J. Hazard. Mater. 360 (2018) 257–269.
[11] S.A. McMaster, R. Ram, F. Charalambous, M.I. Pownceby, J. Tardio, S.K. Bhargava, J. Hazard. Mater. 280 (2014) 478–486.
[12] K.E. Sickafus, R.W. Grimes, J.A. Valdez, A. Cleave, M. Tang, M. Ishimaru, S. M. Corish, C.R. Stanek, B.P. Uberuaga, Nat. Mater. 6 (3) (2007) 217–223.
[13] L. Minervini, R.W. Grimes, K.E. Sickafus, J. Am. Ceram. Soc. 83 (8) (2000) 1873–1878.
[14] J. Lian, R.C. Ewing, L.M. Wang, K.B. Helean, J. Mater. Res. 19 (5) (2011) 1575–1580.
[15] J. Gild, Y. Zhang, T. Harrington, S. Jiang, T. Hu, M.C. Quinn, W.M. Mellor, N. Zhou, K. Vecchio, J. Luo, Sci. Rep. 6 (1) (2016) 1–10.
[16] J. Dusza, P. Švec, V. Girman, R. Sedlák, E.G. Castle, T. Csanádi, A. Kovalčíková, M. J. Reece, J. Eur. Ceram. Soc. 38 (12) (2018) 4303–4307.
[17] T. Jin, X. Sang, R.R. Unocic, R.T. Kinch, X. Liu, J. Hu, H. Liu, S. Dai, Adv. Mater. 30 (23) (2018), 1707512.
[18] J. Gild, M. Samiee, J.L. Braun, T. Harrington, H. Vega, P.E. Hopkins, K. Vecchio, J. Luo, J. Eur. Ceram. Soc. 38 (10) (2018) 3578–3584.
[19] F. Li, S. Li, G. Liu, X. Chen, Y. Wang, J. Nucl. Mater. 513 (2019) 1–7.
[20] Z. Zhao, H. Xiang, F.Z. Dai, Z. Peng, Y. Zhou, J. Mater. Sci. Technol. 35 (11) (2019) 2647–2651.
[21] Z. Zhao, H. Chen, H. Xiang, F.Z. Dai, X. Wang, W. Xu, K. Sun, Z. Peng, Y. Zhou, J. Mater. Sci. Technol. 39 (2020) 167–172.
[22] Z. Teng, Y. Tan, S. Zeng, Y. Meng, C. Chen, X. Han, H. Zhang, J. Eur. Ceram. Soc. 41 (6) (2021) 3614–3620.

[23] V.F. Khokhlov, P.N. Yashkin, D.I. Silin, E.S. Djorova, R. Lawaczeck, in: Y. Mishima (Ed.), Cancer Neutron Capture Therapy, Springer US, Boston, MA, 1996, pp. 865-869.
[24] G. Kresse, J. Furthmüller, Comput. Mater. Sci. 6 (1) (1996) 15–50.
[25] G. Kresse, J. Furthmüller, Phys. Rev. B 54 (16) (1996) 11169–11186.
[26] P.E. Blöchl, Phys. Rev. B 50 (24) (1994) 17953–17979.
[27] J.P. Perdew, K. Burke, M. Ernzerhof, Phys. Rev. Lett. 77 (18) (1996) 3865–3868.
[28] C. Jiang, C. Wolverton, J. Sofo, L.Q. Chen, Z.K. Liu, Phys. Rev. B 69 (21) (2004), 214202.
[29] C. Jiang, C.R. Stanek, K.E. Sickafus, B.P. Uberuaga, Phys. Rev. B 79 (10) (2009), 104203.
[30] J.M. Cowley, Phys. Rev. 77 (5) (1950) 669–675.
[31] M. Li, P. Li, H. Xiao, H. Zhang, X. Zu, J. Nucl. Mater. 542 (2020), 152425.
[32] S.K. Gupta, M. Abdou, P.S. Ghosh, J.P. Zuniga, Y. Mao, ACS Omega 4 (2) (2019) 2779–2791.
[33] B.J. Kennedy, B.A. Hunter, C.J. Howard, J. Solid State Chem. 130 (1) (1997) 58–65.
[34] A.R. Kopan, N.P. Gorbachuk, S.M. Lakiza, Y.S. Tischenko, D.S. Korablov, Powder Metall. Met. Ceram. 57 (5) (2018) 336–343.
[35] B. Mandal, A. Banerji, V. Sathe, S. Deb, A. Tyagi, J. Solid State Chem. 180 (10) (2007) 2643–2648.
[36] K. Nakamura, M. Mori, T. Itoh, T. Ohnuma, AIP Adv. 6 (11) (2016), 115003.
[37] X. Wang, H. Xiao, X. Zu, W.J. Weber, J. Nucl. Mater. 419 (1-3) (2011) 105–111.
[38] Y. Wang, Y. Li, C. Liu, X. Liu, Nucl. Instr. Methods in Phys. Res. Sect. B Beam Interact. Mater. Atoms 436 (2018) 211–216.
[39] S. Zhao, J. Am. Ceram. Soc. 104 (4) (2021) 1874–1886.
[40] C. Liu, Y. Li, Y. Li, L. Dong, J. Wen, D. Yang, Q. Wei, P. Yang, J. Nucl. Mater. 500 (2018) 72–80.
[41] L. Chen, X. Su, Y. Li, Open Access Library J. 1 (3) (2014) 1–8.
[42] N. Li, H. Xiao, X.T. Zu, L.M. Wang, R.C. Ewing, J. Lian, F. Gao, J. Appl. Phys. 102 (6) (2007), 063704.
[43] Y. Li, P.M. Kowalski, G. Beridze, A.R. Birnie, S. Finkeldei, D. Bosbach, Scr. Mater. 107 (2015) 18–21.
[44] F. Zhang, J. Wang, J. Lian, M. Lang, U. Becker, R. Ewing, Phys. Rev. Lett. 100 (4) (2008), 045503.
[45] K. Yang, K. Bryce, W. Zhu, D. Zhao, J. Lian, J. Eur. Ceram. Soc. 41 (4) (2021) 2870–2882.
[46] C. Lu, T. Yang, L. Niu, Q. Peng, K. Jin, M.L. Crespillo, G. Velisa, H. Xue, F. Zhang, P. Xiu, Y. Zhang, F. Gao, H. Bei, W.J. Weber, L. Wang, J. Nucl. Mater. 509 (2018) 237–244.
[47] Y. Li, R. Li, Q. Peng, S. Ogata, Nanotechnology 31 (42) (2020), 425701.
[48] V. Chernyshev, V. Petrov, A. Nikiforov, Phys. Solid State 57 (5) (2015) 996–1002.
[49] J. Feng, B. Xiao, Z.X. Qu, R. Zhou, W. Pan, Appl. Phys. Lett. 99 (20) (2011), 201909.
[50] M. Sun, Y. Sui, K. Gao, C. Tan, L. Dai, G. Zhou, Y. Zhang, L. Wang, J. Ceram. Soc. Jpn. 127 (10) (2019) 722–727.
[51] W. Voigt, Ann. Phys. 274 (12) (1889) 573–587.
[52] A. Reuss, ZAMM J.Appl. Math. Mech. Z. Angew. Math. Mech. 9 (1) (1929) 49–58.
[53] R. Hill, Proceedings of the Physical Society. Section A 65(5) (1952) 349-354.
[54] S.F. Pugh, J. Sci. 45 (367) (1954) 823–843.
[55] M.E. Fine, L.D. Brown, H.L. Marcus, Scr. Metall. 18 (9) (1984) 951–956.